ISSN (Print) 1226-1750
ISSN (Online) 2233-6656
Journal of Magnetics 23(1), 117-124 (2018) https://doi.org/10.4283/JMAG.2018.23.1.117

Preliminary Validation of Robotic Control of Magnetic Particles for Targeted Hyperthermia

Haye Min Ko[1]* and Sung Hoon Kim[2]*

[1]*Department of Bio-Nano Chemistry, Wonkwang University, Jeonbuk 54538, Republic of Korea*
[2]*Department of Electronics Convergence Engineering, Wonkwang University, Jeonbuk 54538, Republic of Korea*

(Received 30 October 2017, Received in final form 9 March 2018, Accepted 12 March 2018)

In this paper, we present a new method for targeted hyperthermia using an electromagnetic navigation system. Typically, Fe_3O_4 magnetic nanoparticles (MNPs) are utilized by injection methods. However, the study demonstrated that the proposed method provides active locomotion for targeting a destination within a three-axis Helmholtz coil, and generates heat through a high-frequency heating coil. To realize these two functions, the entire system combined the electromagnetic navigation system and a high-frequency heating system. The Fe_3O_4 MNPs were prepared via chemical synthesis. Using vibrating sample magnetometer (VSM) and X-ray diffraction (XRD), we observed the magnetic properties and structure of the crystals. Through various experimental tests, we investigated the controllability, mobility, and steering ability of the MNPs. In particular, we confirmed the heating characteristics of the fabricated MNPs according to the changes in the magnetic field strength at 205 kHz. On average, the particle cluster generated a temperature of 73.12 °C at 58 kA/m.

Keywords : active locomotion, hyperthermia, Fe_3O_4 MNPs, electromagnetic navigation system, high-frequency heating system

1. Introduction

Electromagnetic navigation systems are innovative approaches for micro-/nano-robots for diagnosis and therapy in medicine [1-4]. An electromagnetic navigation system for micro-/nano-robot control provides wireless control, battery-free operation, and minimally invasive treatment inside the human body employing external magnetic fields [5-7]. Various microrobots were applied in vascular disease treatment, cancer treatment, and targeted drug delivery previously [8-11]. Typically, an electromagnetic navigation (manipulation) system can provide two types of magnetic fields: gradient or uniform. A gradient magnetic field causes a magnetic force for translational motion, whereas a uniform magnetic field causes rotational motion by generating a magnetic torque. In the case of magnetic torque control, magnetic micro-/nano-robots can generate rolling, rotating, and oscillating motions for active locomotion [12-14]. In particular, owing to the magnetic properties and active locomotion of micro-/nano-robots, magnetic nanoparticles (MNPs) can be applied to targeted drug delivery systems and in scenarios involving hyperthermia. In general, iron oxide (Fe_3O_4) particles are widely used for hyperthermia [15-18]. Normal hyperthermia, which uses external heat, can destroy normal cells. The use of magnetic particles for local hyperthermia can avoid this problem. In addition, it is difficult to inject magnetic particles using a syringe into a location deep within the body. To overcome these issues, we proposed a new approach for targeted hyperthermia based on robotic control using an electromagnetic navigation system. In this study, we fabricated Fe_3O_4 MNPs for robotic control with hyperthermia.

Using vibrating sample magnetometer (VSM) and X-ray diffraction (XRD), we analyzed the magnetic properties and structure of crystal. Furthermore, we investigated the mobility and steering ability of the magnetic particles through experiments. Finally, we verified both the active locomotion based on rolling motion and the function of the targeted hyperthermia using both the navigation coil and the high-frequency heating coil.

In these experiments, we used the total weight of the magnetic particle cluster to conduct the performance

*Co-Corresponding author: Tel: +82-63-850-6739
Fax: +82-63-850-6739, e-mail: kshoon@wku.ac.kr
Tel / Fax: +82-63-850-6229, e-mail: hayeminko@wku.ac.kr

evaluation of active locomotion with targeted hyperthermia.

The total weight of the particle clusters was 0.0525 g, and it took 12 min to move 4 cm under the driving conditions of 5 kA/m and 1 Hz. After the entire cluster arrived at the destination, a high-frequency magnetic field of 205 kHz and 56 kA/m was applied to heat generation. Consequently, the average temperature of the cluster for 200 s was 67 °C, and the peak temperature was observed to be 83 °C. Various experimental analyses were performed to verify the proposed method.

2. Synthesis and Principle of Robotic Control of Magnetic Particles

2.1. Synthesis of the iron oxide (Fe_3O_4) magnetic particles

Iron (II) chloride tetrahydrate ($FeCl_2 \cdot 4H_2O$) and iron (III) chloride hexahydrate ($FeCl_3 \cdot 6H_2O$) were purchased from Wako chemicals. Sodium hydroxide was purchased from Samchun chemicals. To provide ultrapure water, water was distilled by a Q-Grad 1 purification cartridge from Millipore water purification systems. Following the general procedure, iron (II) chloride tetrahydrate (2.65 g, 13.32 mmol) and iron (III) chloride hexahydrate (7.208 g, 26.66 mmol) were dissolved in ultrapure water (200 ml). After stirring at room temperature for 10 min, sodium hydroxide (NaOH, 9.6 g, 0.24 mol) in ultrapure water (40 ml) was added, which immediately led to the formation of a black precipitate, and the reaction mixture was stirred for 30 min. This process is described by the chemical equation below:

$$Fe^{2+} + 2Fe^{3+} + 8OH^- \rightarrow Fe_3O_4 + 4H_2O \quad (1)$$

This black precipitate was separated by filtration and washed with ultrapure water until a neutral pH was obtained. The iron oxide nanoparticles were dried by an evaporator, and the residue water was concentrated under reduced pressure at 70 °C for 20 h.

2.2. Principle of magnetic remote control for active locomotion

For active locomotion, we utilize an electromagnetic navigation system based on a three-axis Helmholtz coil. The coil system generates a uniform rotating magnetic field that produces magnetic torque with magnetic particles for active locomotion. The generated magnetic torque results in a rolling motion of magnetic particles. When the applied magnetic field aligns magnetic cluster and forms a chain, as shown in Fig. 1(a) and (b). The rotating magnetic field causes a rolling motion of the magnetic chain by magnetic torque. The magnetic torque can be expressed as follows:

$$\boldsymbol{T} = \mu_0 \boldsymbol{m} \times \boldsymbol{H}, \quad (2)$$

where μ_0 is the permeability of free space, and $\boldsymbol{m}$ and $\boldsymbol{H}$ are the magnetic moment and magnetic field strength,

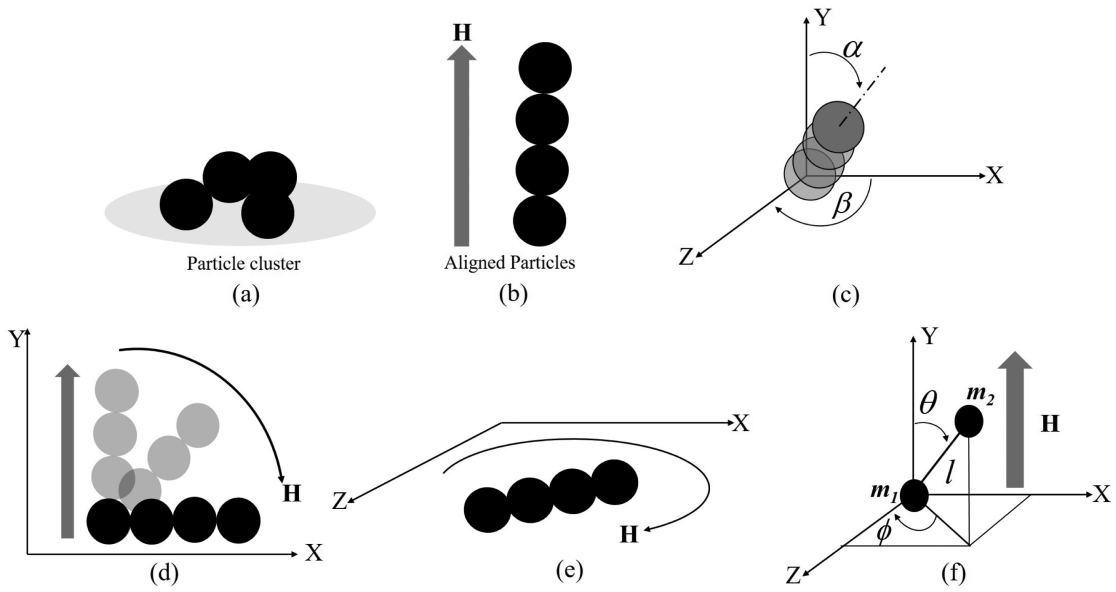

Fig. 1. Principle of magnetic actuation by external magnetic fields: (a) magnetic particle cluster. (b) The aligned magnetic particles by the direction of the external magnetic field. (c) Method of 3D motion control using the control of the angles of α and β. (d) Rolling motion on XY plane by the rotating magnetic field. (e) Rotation of the chain on XZ plane by rotating magnetic field. (f) The spatial position of a magnetic dipole pair in the 3D coordinate system.

respectively. Figure 1(c) shows a steering mechanism with a rolling motion of the magnetic chain in a three-axis magnetic navigation system. The steering angles α and β are the zenith and azimuth angles of the plane of the magnetic field, respectively. The two angles control the direction of the rolling motion due to magnetic torque. If we consider 3D control of the magnetic chain, the applied magnetic field can be expressed as follows:

$$\boldsymbol{H}_{x,y,z} = \begin{pmatrix} \boldsymbol{H}_x \\ \boldsymbol{H}_y \\ \boldsymbol{H}_z \end{pmatrix} = \boldsymbol{H}_0 \begin{pmatrix} \cos\beta \sin\alpha \sin\omega\boldsymbol{t} - \sin\beta \cos\omega\boldsymbol{t} \\ \cos\beta \cos\omega\boldsymbol{t} + \sin\beta \sin\alpha \sin\omega\boldsymbol{t} \\ \cos\alpha \sin\omega\boldsymbol{t} \end{pmatrix}, \quad (3)$$

where H_0 is the field strength: $\boldsymbol{H}_0 = niR^2/(R^2 + x^2)^{3/2}$, n is the number of coil turns, i is the current in amperes and D and x are the radius of the Helmholtz coil and the distance between one pair of Helmholtz coils, respectively. When the magnetic moment vector $\boldsymbol{m}$ rotates in the YZ plane, $\boldsymbol{m}$ = (0, $\boldsymbol{m}_0 \cos\theta$, $\boldsymbol{m}_0 \sin\theta$). Thus, the driving torque of the magnetic chain for steering can be expressed as follows:

$$\boldsymbol{T} = \mu_0 \boldsymbol{m} \times \boldsymbol{H}_{x,y,z}$$

$$\boldsymbol{T} = \mu_0 \boldsymbol{m}_0 \boldsymbol{H}_0 \begin{Bmatrix} (\cos\alpha \cos\theta \sin\omega\boldsymbol{t} - \sin\theta(\cos\beta \cos\omega\boldsymbol{t} \\ + \sin\beta \sin\alpha \sin\omega\boldsymbol{t}))\boldsymbol{i} \\ -\sin\theta(\sin\beta \cos\omega\boldsymbol{t} - \cos\beta \sin\alpha \sin\omega\boldsymbol{t})\boldsymbol{j} \\ +\cos\theta(\sin\beta \cos\omega\boldsymbol{t} - \cos\beta \sin\alpha \sin\omega\boldsymbol{t})\boldsymbol{k} \end{Bmatrix}. \quad (4)$$

When the plane of the rotating magnetic field is the XY plane, the magnetic chain moves along the X-axis, as shown in Fig. 1(d). In addition, when the plane of the magnetic field is plane XZ, the magnetic chain rotates in place because the rotating axis becomes the Z-axis, as shown in Fig. 1(e). For robotic control of magnetic particles, we utilized a uniform rotating magnetic field and controlled the direction of magnetic torque. This method is defined as magnetic torque control. Figure 1(f) shows the spatial position of a magnetic dipole pair in the 3D coordinate system. Here, we consider the interaction energy between two magnetic dipoles as follows:

$$\boldsymbol{E}_{m_1,m_2} = \frac{1}{4\pi\mu \boldsymbol{r}^3}[\boldsymbol{m}_1\boldsymbol{m}_2 - 3(\boldsymbol{m}_1 \cdot \boldsymbol{c}_r)(\boldsymbol{m}_2 \cdot \boldsymbol{c}_r)], \quad (5)$$

where μ denotes the medium permeability, $\boldsymbol{r}$ denotes the distance between magnetic dipoles, and $\boldsymbol{c}_r$ is the unit vector of the center between magnetic dipoles. If the magnetic dipoles have the same properties, the interaction energy is $\boldsymbol{E}_{m,m} = \boldsymbol{m}^2(1-3\cos^2\theta)/4\pi\mu|\boldsymbol{r}|^3$. We can obtain force equation from the interaction energy because a partial derivative of energy is defined as force.

When the distance between magnetic particles is large, mutual magnetization is negligible. However, if the distance is relatively short, the mutual magnetization will affect the magnetic dipole's magnetic moment. When we consider mutual magnetization, the magnetic moment of the dipoles can be expressed as follows [19]:

$$\boldsymbol{m} = \left\{ \begin{array}{l} \boldsymbol{m}_x = 12\pi\mu {R_m}^3 \boldsymbol{H} \left(\dfrac{\mu_k - \mu_r}{\mu_k + 2\mu_r} \right)^2 \Big/ \\ \qquad (\boldsymbol{r}^2 + {R_m}^2)^{5/2} \left(1 - \dfrac{4\pi\mu {R_m}^3 (\mu_k - \mu_r)}{\mu_k + 2\mu_r} \right) \\ \boldsymbol{m}_y = 4\pi\mu xy {R_m}^6 \boldsymbol{H} \left(\dfrac{\mu_k - \mu_r}{\mu_k + 2\mu_r} \right)^2 \Big/ \\ \qquad \left(1 - \dfrac{4\pi\mu {R_m}^3 (\mu_k - \mu_r)}{\mu_k + 2\mu_r} \right) \\ \boldsymbol{m}_z = 12\pi\mu yz {R_m}^6 \boldsymbol{H} \left(\dfrac{\mu_k - \mu_r}{\mu_k + 2\mu_r} \right)^2 \Big/ \\ \qquad (\boldsymbol{r}^2 + {R_m}^2)^{5/2} \left(1 - \dfrac{4\pi\mu {R_m}^3 (\mu_k - \mu_r)}{\mu_k + 2\mu_r} \right) \end{array} \right\}, \quad (6)$$

where μ_k and μ_r are the relative permeability of the magnetic particles and the medium, respectively, R_m is the radius of the magnetic dipole, and $\boldsymbol{H}$ is the applied magnetic field. Force can be expressed as a partial derivative of energy. In Fig. 1(f), substituting $x/l = \sin\theta\cos\phi$, $y/l = \sin\theta\cos\phi$, $z/l = \cos\theta$, and $l = \sqrt{x^2 + y^2 + z^2}$ into Eq. (6). Therefore, the force equation can be expressed by Equation (7) by applying a partial differentiation to the x, y, and z elements in the energy equation.

$$\begin{aligned} \boldsymbol{F}_x &= \frac{|\boldsymbol{m}_x|^2 \, 3(5\cos^2\theta - 1)\sin\theta\sin\phi}{4\pi\mu \boldsymbol{r}^4} \\ \boldsymbol{F}_y &= \frac{|\boldsymbol{m}_y|^2 \, 3(5\cos^2\theta - 3)\cos\theta}{4\pi\mu \boldsymbol{r}^4} \\ \boldsymbol{F}_z &= \frac{|\boldsymbol{m}_z|^2 \, 3(5\cos^2\theta - 1)\sin\theta\cos\phi}{4\pi\mu \boldsymbol{r}^4} \end{aligned}. \quad (7)$$

Figure 2 shows the developed electromagnetic navigation system with a high-frequency heating coil. The system consists of three-axis Helmholtz coil, Labview-based control software, and three power supplies. The fabricated coil generates a uniform magnetic field at 20 cm × 20 cm × 20 cm. The number of turns of x, y and z coil is 960, 1200, and 760, respectively. The inner diameter and number of turns of the heating coil were 6 cm and 4 turns, respectively. For the generation of high frequency magnetic fields, the driving power supply is adjustable up to 5 kW.

Figure 3(a) shows the magnetic fled strength at the

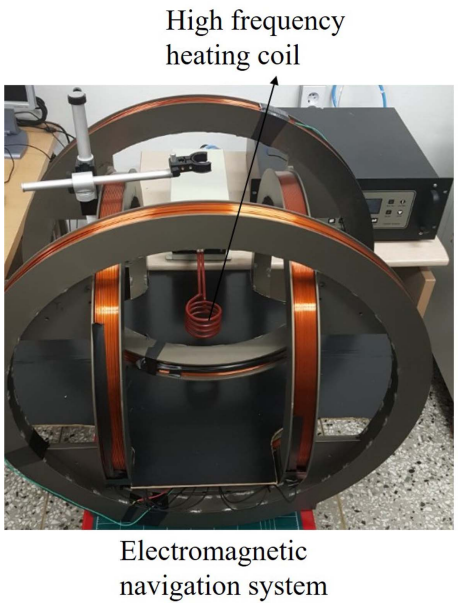

Fig. 2. (Color online) Total coil system: three-axis Helmholtz coil for an electromagnetic navigation system (control of active locomotion with steering) and a high-frequency heating coil for targeted hyperthermia.

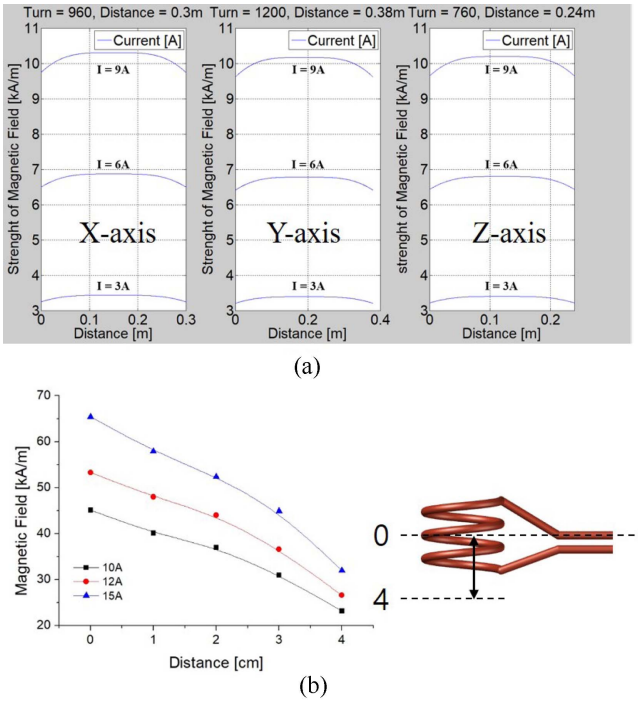

Fig. 3. (Color online) (a) Calculated magnetic field strength for three-axis Helmholtz coils according to changes in the applied currents. (b) Magnetic field distribution of the heating coil according to changes in the distance and the currents of 10, 12, and 15 A at coil center to the 4-cm points.

three coils. The applied currents of 3, 6, and 9 A generate the uniform magnetic fields of 3.4, 6.8, and 10.2 kA/m, respectively. Figure 3(b) shows the magnetic field strength of the high-frequency heating coil according to changes in the driving currents (10 A, 12 A, and 15 A at a driving frequency of 208 kHz). Under these conditions, the heating coil generates a magnetic field strength of 38.4, 48.3, and 57 kA/m at the center of the heating coil. In addition, the coil generates 9.7, 10.4, and 12.6 at 4 cm from the center of the coil, respectively.

2.3. Targeted hyperthermia

For the targeted hyperthermia, we utilized an additional high-frequency heating coil. When we control the magnetic particles, we use an electromagnetic navigation system based on a three-axis Helmholtz coil. When the magnetic particles reach the target point, the navigation system is stopped, and the high-frequency heating coil is driven for the targeted hyperthermia. For hyperthermia, the driving range of the magnetic field strength is up to 57 kA/m at 208 kHz. The heating temperature is observed by a thermal imaging camera. Figure 2 shows the inclusion of a heating coil in the electromagnetic navigation system for targeted hyperthermia.

3. Experimental Analysis

To verify the remote control (active locomotion) with the function of heat generation, various experimental analyses using the magnetic navigation system with a high-frequency heating system were conducted. First, we observed the magnetic properties and the X-ray diffraction pattern of the fabricated magnetic particles using VSM and XRD, respectively, as shown in Fig. 4. The fabricated sample represented a magnetization of 53.747 emu/g and a coercive force of 5.1452 Oe. In addition, the fabricated magnetic particles reveal diffraction peaks at (111), (220), (311), (400), (422), (511), (400), etc. These are characteristic peaks of the Fe_3O_4 crystal with a cubic spinel structure. The average size of the fabricated particles is 10-25 um, which is calculated by XRD analysis.

Second, we verified the remote control with active locomotion of the magnetic cluster within the electromagnetic navigation system for the targeted hyperthermia. For active locomotion, we conducted three tests: rolling motion, rotation, and steering. In addition, these experiments were conducted at a driving frequency of up to 30 Hz in the range of magnetic field strengths of 3-9 kA/m. Figure 5 shows the sizes of the magnetic chain at the applied fields of 3, 6, and 9 kA/m with the fixed 1 Hz. The results are the average of ten chain lengths in ten measurements. The length of the magnetic chain is proportional to the applied field strength at the constant

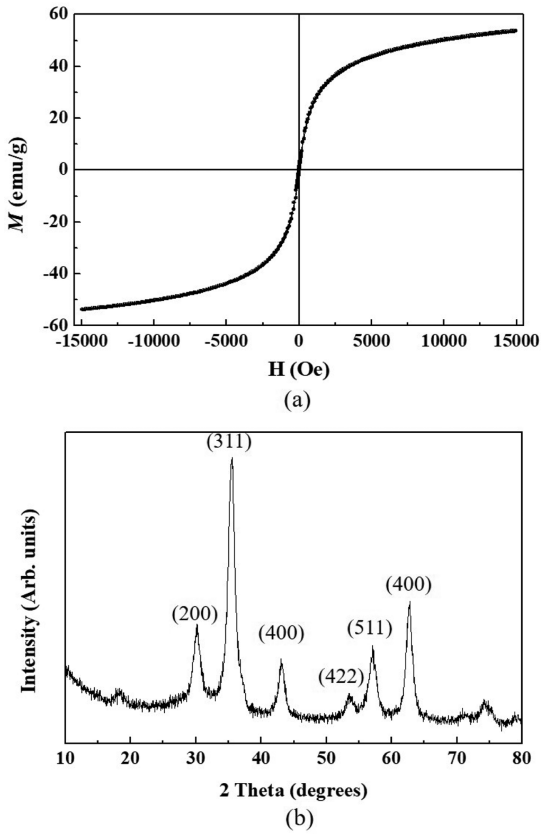

Fig. 4. (a) Magnetic properties of the fabricated Fe_3O_4 magnetic particles by VSM measurement and (b) structure of crystal analysis by XRD.

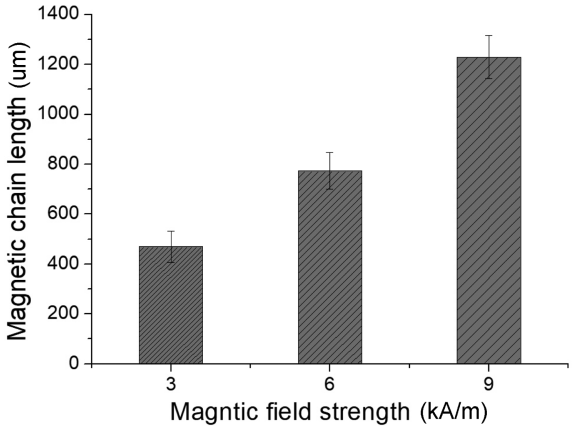

Fig. 5. The average lengths of the magnetic chain at 3, 6, and 9 kA/m with the fixed 1 Hz.

frequency. The applied fields of 3, 6, and 9 kA/m caused the average length of approximately 470, 773, and 1229 um, respectively.

Figure 6(a) shows the rolling motion of the magnetic chain according to changes in the position of rotating magnetic field from 180 degrees to 0 degree. The rolling motion was conducted at a magnetic field strength of 7 kA/m and a frequency of 0.5 Hz within the XY plane. The starting angle was 180 degrees, and the rotating direction of the magnetic field was clockwise. For the stable rolling motion of the particles (magnetic chain), a

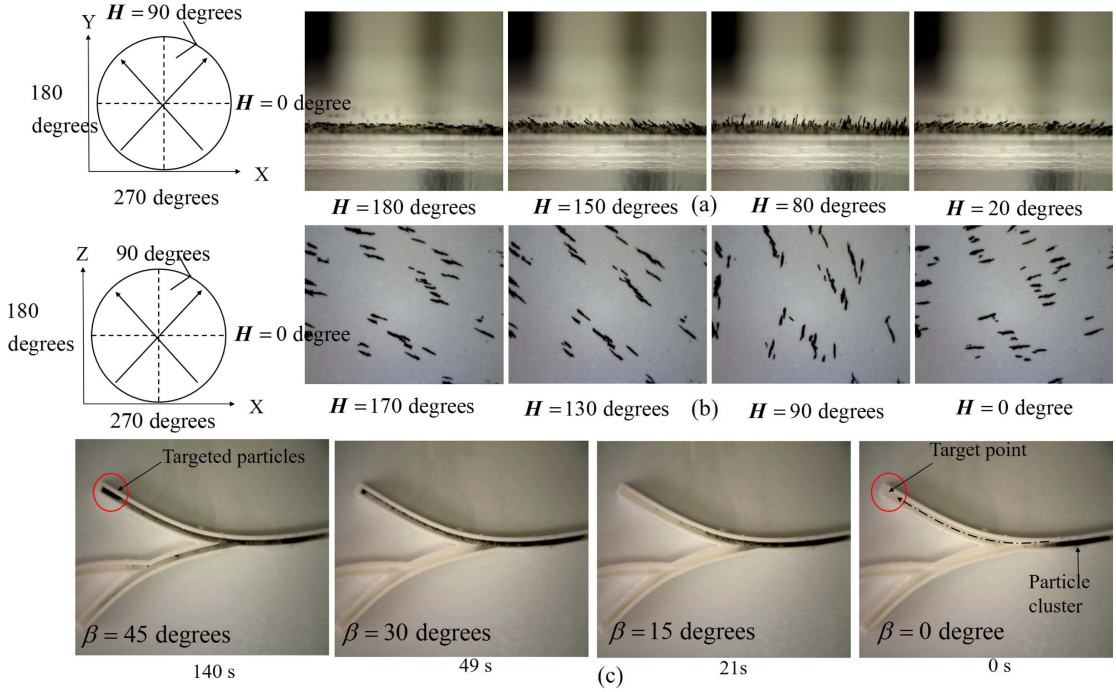

Fig. 6. (Color online) Results of active locomotion: (a) rolling motion of magnetic chain at the rotating magnetic field in the XY plane, (b) rotating motion at the rotating magnetic field in the XZ plane, and (c) active locomotion with steering according to changes in the angel of β up to 45 degrees.

minimum magnetic field strength of 4.5 kA/m is required, and the driving frequency must be the maximum 10 Hz, because a maximum of 30 Hz becomes a step-out point, which causes separation of the straight chain at 4.5 kA/m. The magnetic field strength of 7 kA/m generated a step-out point at the driving frequency of 60 Hz in the test. Figure 6(b) shows the rotation of magnetic chain according to the changes in the position of the magnetic field in the YZ plane. To change the plane of a rotating magnetic field from the XY plane to the XZ plane, we adjust the control angle of α from 90 degrees to 0 degree. The driving conditions of rotating motion are equivalent to the test of rolling motion. The magnetic chains rotated in place without lateral movement. Figure 6(c) shows the rolling-motion-based active locomotion with steering at the driving condition of 7 kA/m and 2 Hz. The total amount of magnetic particles used in the test was 0.0525 g. The length of the travel path is 8 cm, and the angle of destination is 45 degrees. Therefore, the steering angle β was gradually increased to 45 degrees (0, 15, 30, and 45 degrees), and the angle α is a constant 90 degrees to reach the destination. It took 140 seconds for all the magnetic particles to reach at the destination. The developed electromagnetic navigation provides 3-dimensional active locomotion using the two control angles of α and β.

Figure 7 shows the active locomotion of a ball magnet chain by the angles (α and β) for 1 period in silicone oil of 3000 cst. We used permanent magnets instead of magnetic particles because the size of the magnetic particle chains was small when rotated in the X, Y, and Z direction and it is difficult to measure with a photograph. In this experiment, the driving frequency was 0.5 Hz

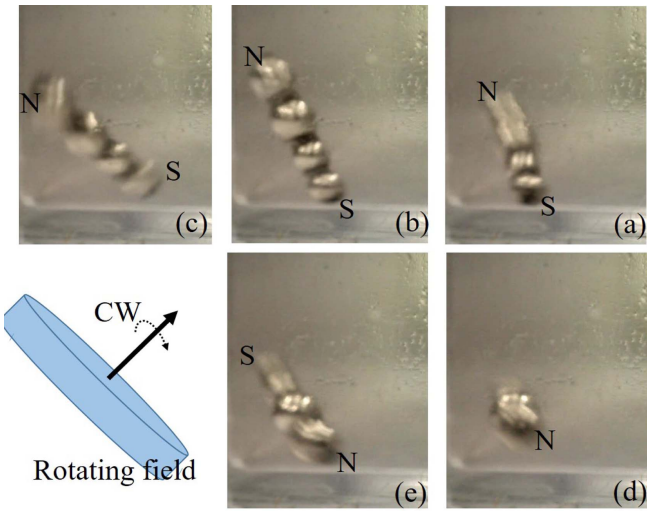

Fig. 7. (Color online) 3D rolling motion in the 3D coordinate system at the control angles of α (60 degrees) and β (40 degrees) for 1 period in silicone oil of 3000 cst.

Fig. 8. (Color online) Observing the shape of the magnetic chain in the rotating motion according to the driving frequency: (a) the aligned magnetic chain at 3 Hz and (b) separation of the aligned magnetic chain at 30 Hz.

(clockwise) and the applied magnetic field strength was 3 kA/m. The plane of the rotating magnetic field was transformed from the 2D coordinate system to the 3D coordinate system by α (60 degrees) and β (40 degrees). The angle α determines the up/down steering of the magnetic chain, whereas the angle β determines the left and right steering. In particular, we investigated the form of the magnetic chain according to changes in the driving frequency. Magnetic particles are aligned by an external magnetic field, resulting in two forms: fanning or coherent. Fanning is that the $\boldsymbol{M}_s$ vectors of successive spheres in the chain fan out in a plane by rotating in the alternate direction in alternate spheres. Coherent is that the $\boldsymbol{M}_s$ vectors of all the spheres are always parallel.

The aligned magnetic chains are able to maintain their forms at low frequency during rolling motion, whereas the forms of the chain cannot be maintained at high frequency, because the rotational kinetic energy is higher than the magnetostatic energy of the chain at high frequency. Figure 8 shows the observed form of the magnetic chain at driving frequencies of 3 Hz and 30 Hz within 4.5 kA/m. The applied magnetic field at 3 Hz was able to maintain the straight magnetic chain, whereas the straight magnetic chain was broken at a driving frequency of 30 Hz.

To verify the performance of the targeted hyperthermia, we conducted an observation of the basic heating property using the high-frequency heating coil at the driving magnetic fields of 38, 48, and 58 kA/m at 205 kHz for 600 seconds, as shown in Fig. 9(a). Under these conditions, the fabricated magnetic particles (0.0525 g) were installed at the center of the heating coil, and we measured the mean value of the heat generation from the particle distribution area. The average temperature of each applied field was measured as 62.64 °C, 68.52 °C, and 73.12 °C. Figure 9(b) shows the result of heat gene-

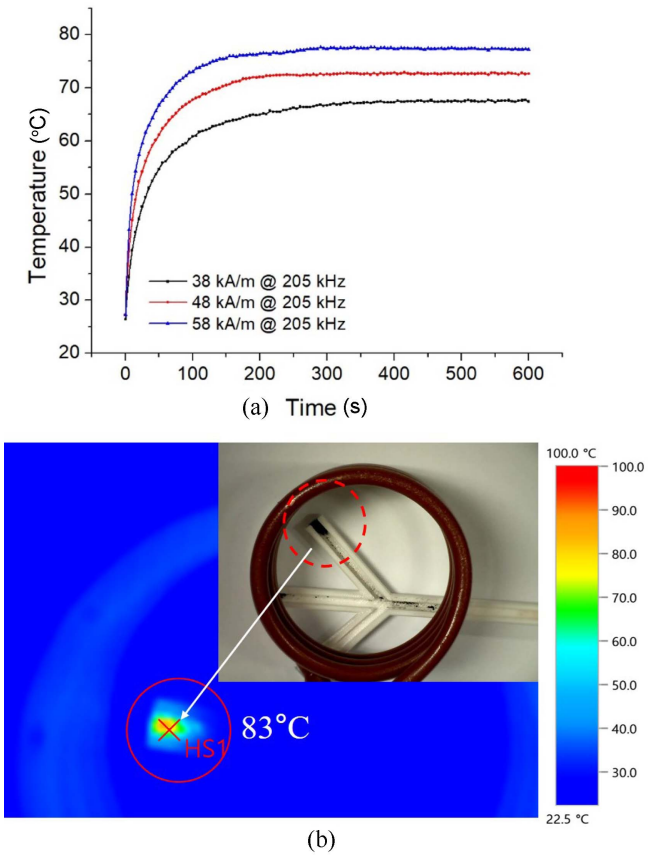

Fig. 9. (Color online) Observation of heat generation for hyperthermia: (a) heating temperature inside heating coil according to changes in the applied magnetic field at 205 kHz and (b) when a high-frequency magnetic field was applied for 200 s after targeting. HS refers to the hot spot on the thermal image.

ration after targeting using a thermal imaging camera. The experiment uses both the electromagnetic navigation system for targeting and the high-frequency heating coil. First, the particles are moved to the destination with a magnetic field of 5 kA/m and a driving frequency of 1 Hz from the electromagnetic navigation system, and the heat is generated by a high-frequency heating coil at a driving frequency of 205 kHz with the magnetic field of 58 kA/m. The length of the destination path was 4 cm and the entire particle took 12 minutes to move to the destination. After all the particles were moved to the destination, the magnetic field of the navigation system was stopped, and we generated a high-frequency magnetic field from the heating coil for 200 seconds to observe the heat generation. After 200 seconds, the average temperature of the distribution area of the particle cluster was 67 °C, and the peak temperature was 83 °C, as shown in Fig. 9(b).

4. Discussion and Conclusion

In this study, a robotic control of magnetic particles for targeted hyperthermia based on the combined electromagnetic navigation system with a high-frequency heating system was proposed. The magnetic particles, which are controlled by an external rotating magnetic field, performed active locomotion, steering, and heating. In addition, we observed the magnetic properties and structure of crystal through VSM and XRD analysis. The magnetic particles showed a straight alignment (chain) in the external magnetic field. Because the straight chains were synchronized by the applied rotating magnetic field, the straight chains generated rolling and rotating motions according to changes in the plane of the rotating magnetic field. Because the prepared particles had a low magnetization of 53.747 emu/g, the external driving magnetic field showed stable active locomotion from 4.5 kA/m. In particular, the driving frequency determined the form of the particle chain. In this experiment, the form of the straight chain was partially maintained until 15 Hz, and was completely separated at 30 Hz or more. Thus, a low driving frequency is required to maintain the rolling motion in the form of a straight chain. The particles were targeted to the destination with an external rotating magnetic field, and a heat-generation experiment was performed in the magnetic field strength range of 38-58 kA/m at 205 kHz using a high-frequency magnetic heating system. Heat generation was performed in the atmosphere, and the peak temperature was observed at 83 °C for 200 s. Through various experiments, we were able to confirm the possibility of targeted hyperthermia based on robotic control. The phantom model, which is similar to the human body model, will be developed and tested to validate the proposed method. In addition, we will experimentally verify particle motion, heat generation, etc. in the fluid environment.

Acknowledgments

This research was supported by Wonkwang University in 2016.

References

[1] J. J. Abbott, K. E. Peyer, M. C. Lagomarsino, L. Zhang, L. X. Dong, I. K. Kaliakatsos, and B. J. Nelson, Int. J. Robot. Res. **28**, 1434 (2009).
[2] A. Ghosh and P. Fischer, Nano Lett. **9**, 2243 (2009).
[3] B. J. Nelson, I. K. Kaliakatsos, and J. J. Abbott, Annu.

Rev. Biomed. Eng. **12**, 55 (2010).
[4] C. H. Yu and S. H. Kim, J. Mag. **22**, 162 (2017).
[5] K. Ishiyama, M. Sendoh, and K. I. Arai, JMMM. **242-245**, 41 (2002).
[6] S. H. Kim, S. Hashi, and K. Ishiyama, J. Appl. Phys. **109**, 07E318 (2011).
[7] S. H. Kim and K. Ishiyama, IEEE Trans. Mechatron. **19**, 1651 (2013).
[8] L. Sadelli, M. Fruchard, and A. Ferreira, IEEE Trans. Automatic Control. **62**, 2194 (2017).
[9] J. Han, V. D. Nguyen, G. Go, Y. Choi, S. Y. Ko, and J. O. Park, Scientific Reports **6**, 28717 (2016).
[10] H. Li, G. Go, S. Y. Ko, J. O. Park, and S. Park, Smart Mater. Struct. **25**, 027001 (2016).
[11] L. Zhang, J. Abbott, L. Dong, K. D. Bell, and B. J. Nelson, Appl. Phys. Lett. **94**, 064017 (2009).
[12] M. T. Hou, H. M. Shen, G. L. Jiang, C. L. Lu, I. J. Hsu, and J. A. Yeh, J. Appl. Phys. **96**, 024102 (2010).
[13] F. Qiu and B. J. Nelson, Engineering **1**, 21 (2015).
[14] S. H. Kim, J. Y. Lee, S. Hashi, and K. Ishiyama, Robotics and Autonomous System **60**, 288 (2012).
[15] L. M. Bauer, S. F. Situ, M. A. Griswold, and A. C. S. Samia, Nanoscale **8**, 12162 (2016).
[16] K. D. Bakoglidis, K. Simeonidis, D. Sakellari, G. Stefanou, and M. Angelakeris, IEEE Trans. Magnetics **48**, 1320 (2012).
[17] L. Laurent, S. Dutz, U. Hafeli, and M. Mahmoudi, Adv. Colloid Interface **166**, 8 (2011).
[18] M. Kallumadil, M. Tada, T. Nakagawa, M. Abe, P. Southern, and Q. A. Pankhurst, J. Magn. Magn. Mater. **321**, 1509 (2009).
[19] J. G. Ku, X. Y. Liu, H. H. Chen, R. D. Deng, and Q. X. Yan, AIP Adv. **6**, 025004 (2016).